RSC Advances

PAPER

View Article Online
View Journal | View Issue

Cite this: *RSC Adv.*, 2025, **15**, 5316

Photocatalytic hydrocarbon production from aqueous acetic acid using TiO_2 with simultaneous photodeposition of Cu†

Monir Uzzaman, *[a] Mai Furukawa,[a] Ikki Tateishi,[b] Hideyuki Katsumata, [a] Mst. Farhana Afrin[a] and Satoshi Kaneco*[a]

Photocatalytic techniques are considered clean, sustainable and cost-effective in energy conversion and environmental restoration. The large band gap, light harvesting limitation and rapid electron–hole pair recombination can suppress the photocatalytic efficiency in photocatalytic applications. Metal deposition has become one of the most important technical means to improve photocatalytic efficiency. This study has dealt with photocatalytic hydrocarbon and hydrogen production from the acetic acid solution with simultaneous *in situ* Cu deposition on TiO_2 photocatalyst surface. Due to having favorable redox potential and work function values, the photodeposition and Schottky junction formation of Cu occurred smoothly on the TiO_2 surface, which further contributed to accelerating the interfacial charge transfer and photocatalytic activity. The reaction conditions (Cu^{2+} loading, reaction pH and initial concentration of acetic acid) were optimized to enhance photocatalytic methane production. Under the optimum condition, the Cu/TiO_2 photocatalytic hydrocarbon production was maximum (4136 μmol g^{-1}), approximately 9 times better than those obtained with pure TiO_2 (450 μmol g^{-1}). The surface morphological and optical properties of photodeposited Cu/TiO_2 samples were characterized before and after the photocatalytic reaction with utmost precision and thoroughness using a TEM, XPS, DRS, PL, N_2 adsorption–desorption isotherm and BET surface area analysis. The DRS and PL study confirm that *in situ* Cu-deposition on TiO_2 reduced the energy bandgap and improved the light-harvesting area, photogenerated electron–hole pair separation and migration efficiency, respectively. Cycle experiments disclose that the simultaneous Cu-deposited photocatalyst has excellent stability and reusability. A reaction mechanism was proposed for the photocatalytic hydrocarbon formation from the acetic acid by Cu/TiO_2 photocatalytic reaction.

Received 12th December 2024
Accepted 18th January 2025

DOI: 10.1039/d4ra08731c

rsc.li/rsc-advances

1. Introduction

In 2015, the "Paris Agreement" attempted to limit global warming by reducing greenhouse gas emissions, especially carbon dioxide (CO_2) emissions from the burning of fossil fuels (coal, oil and natural gas), the major contributor to climate change.[1] Clean energy sources (solar, wind, hydropower, geothermal, biomass and nuclear energy) can help to establish decarbonization attempts.[2] The utilization of multiple energy resources can release various hazardous and poisonous compounds into the environment.[3] Meanwhile, with the depletion of natural non-renewable energy resources, demand increases for the development of renewable and eco-friendly energy resources.[4] In the past few decades, numerous researches were conducted for the effective ways to the energy demands[5] and environmental remedies.[6] Although there are several ways to produce methane, including natural gas extraction, steam reforming, pyrolysis, anaerobic digestion and Sabatier, the photocatalytic transformation of organic substances is an alluring strategy for the production of hydrocarbons considering the environmental issues.[7] Recently, photocatalytic techniques have been effectively employed in organic synthesis, detoxification, water splitting, nitrogen fixation, CO_2 reduction and energy production due to their readily availability, photostability and less toxicity.[8] They can boost the chemical reaction in the visible, infrared and ultraviolet light ranges.[9] The catalyst's crystal size, surface area, electron–hole pair recombination rate, and applied light wavelength affect its photocatalytic activity.[10,11] A positive hole (h^+) forms as a result of an electron (e^-) moving from the valence band (VB) to the conduction band (CB) when the energy of the irradiation light is equal to or higher than the energy band gap (E_g) of the photocatalyst. Finally, the reduction and oxidation of the target structure are performed by the photogenerated electrons and positive holes.[12]

[a]*Department of Applied Chemistry, Graduate School of Engineering, Mie University, Tsu, Mie 514-8507, Japan. E-mail: monircu92@gmail.com; kaneco@chem.mie-u.ac.jp*
[b]*Mie Global Environment Center for Education & Research, Mie University, Tsu, Mie 514-8507, Japan*

† Electronic supplementary information (ESI) available: Tables S1–S3 and Fig. S1–S5. See DOI: https://doi.org/10.1039/d4ra08731c

TiO_2 has been one of the many semiconductor-based photocatalysts due to its advantageous electrical and optical characteristics, thermodynamic and chemical stability, crystallinity, non-toxicity, resilience to corrosive conditions and comparatively low cost.[13,14] Nevertheless, because of the quick recombination of photogenerated holes and electrons (h^+/e^-) and the high band gap ($E_g = 3.2$ eV), TiO_2 itself works better in the ultraviolet (UV) region only.[15] Metal deposition appears to be a viable strategy to overcome these wavelength limitations, whereby the specific interaction between the metal and TiO_2 determines whether or not the catalysts' characteristics may be improved. The redox potential of Cu is situated between the VB and CB of TiO_2, which allows Cu for smooth deposition on the TiO_2 surface. Similarly, the larger work value of Cu than the TiO_2 favored the Schottky-junction formation and enhanced the photocatalytic efficiency by hindering electron–hole recombination. 1978, Kraeutler and Bard first reported methane production from acetic acid solution using the Pt-loaded TiO_2 photocatalyst.[16] Previously, the insertion of metals (Ag, Au, Pd, Pt, Co, Cu, Mg, Ni, Sn, Fe, Mn, Au, La, Ru and Rh) into the TiO_2 lattice also resulted in a reduction in the energy band gap and a slower rate of (h^+/e^-) recombination.[17–24] Mozia *et al.* reported the physicochemical,[25] suspended[26] and Fe-modified[7,27] effects of TiO_2 photocatalytic decomposition of acetic acid for hydrocarbon evolution under UV light (365 nm) irradiation at room temperature. Heciak *et al.*[28] and Amorós-Pérez *et al.*[29] also reported the Cu-modified TiO_2 catalytic production of biogas (mainly CH_4) and hydrogen under UV light irradiation at room temperature. Asal *et al.* also looked at the synthesis of methane from acetic acid over La^{3+}-modified TiO_2 and found that the output was marginally enhanced under the same reaction conditions, the output was marginally enhanced.[23] Betts *et al.* reported the P25 TiO_2 photocatalytic alkane production from acetic acid and propionic acid.[30] Recently, Cao *et al.* reported significantly enhanced methane production from acetic acid using the platinized TiO_2 under argon and CO_2 conditions.[31] However, combining TiO_2 with inexpensive, readily available metal oxides (Fe_2O_3, SnO_2, Al_2O_3, ZnO, Ag_2O, NiO, Cu_2O and CuO) also significantly enhanced the photocatalytic efficiencies in various magnitudes.[32–41]

The present work mainly focused on photocatalytic hydrocarbon (primarily methane) production from aqueous acetic acid solution employing TiO_2 with *in situ* simultaneous photodeposition of copper under atmospheric conditions. Compared to other reports, the Cu/TiO_2 photocatalyst demonstrated more efficient methane synthesis and the simultaneous Cu deposition on TiO_2 was a relatively straightforward process. Finally, the photocatalytic reaction smoothly proceeded under ultraviolet (365 nm) and visible light (405 nm) irradiation without any noble expensive metals (Ag, Au and Pt).

2. Experimental section

2.1. Materials

All the reagents were analytical grade and used as received without further purification. CH_3COOH (99.7%) and $CuCl_2$ (95.0%) were purchased from FUJIFILM Wako Pure Chemical Corporation, $Cu(CH_3COO)_2 \cdot H_2O$ (99.0%) was purchased from Kanto Chemical Co., Ltd., TiO_2 (P-25) photocatalyst was purchased from Degussa Co., Ltd., Germany (anatase 75%, rutile 25%, surface area 53 $m^2\ g^{-1}$, particle size 25 nm) and CuO (surface area 29 $m^2\ g^{-1}$, particle size 33 nm) was purchased from Sigma-Aldrich Chemicals Pvt. Ltd.

2.2. Characterization

The surface morphology was analyzed by transmission electron microscope on JEM-2100 TEM (JEOL, Japan) and the surface structure characteristic of the products was recorded on X-ray photoelectron spectroscopy PHI Quantera SXM photoelectron spectrometer with Al Kα radiation. Optical properties were inspected by the UV-vis diffuse reflectance sorption (DRS) spectroscopy on the JASCO V-750 UV-vis instrument equipped with an integrating sphere adaptor in the wavelength range of 200–700 nm. Photoluminescence (PL) spectroscopic measurement was carried out by Shimadzu fluorescence spectrometer (RF-5300PC, Japan). The photocatalysts' BET surface area, total pore volume and average pore size were assessed from the N_2 adsorption–desorption isotherm utilizing a BELSORP-miniII (MicrotracBEL) apparatus.

2.3. Photocatalytic methane evolution

All the photocatalytic hydrocarbon and hydrogen production experiments were carried out in a heat resistance Pyrex glass vessel (inner volume: 123 mL). The photocatalyst (50 mg of TiO_2) and co-catalyst (5.6 ppm of CuO, 0.45 wt% of Cu^{2+} relative to the weight of TiO_2) were dispersed in 40 mL of aqueous acetic acid (1.0 M) solution, heated to 50 °C with constant stirring, then illuminated by UV-vis (365 nm, ~12.0 mW cm^{-2}) and visible light (405 nm) for 3 h, respectively. The produced hydrocarbon was examined by gas chromatography (GC-353B, GL Science, Japan) using a flame ionization detector. The column was packed with Porapak Q (mash, 80–100) and the carrier gas was N_2 (99.9%, 29.5 mL min^{-1}). Similarly, the evolved hydrogen and consumed oxygen were analyzed using a gas chromatographer (GL Sciences, GC-3200) equipped with a thermal conductivity detector, with the injection part, column and detector maintained at 50 °C.

3. Results and discussion

3.1. Effect of metallic source on photocatalytic methane production under UV/vis irradiation

The effect of metallic source on photocatalytic methane production from the aqueous solution of acetic acid using TiO_2 with *in situ* simultaneous deposition of copper was studied under UV light (365 nm) irradiation (Fig. 1a). The photocatalytic methane production with pure TiO_2 was 450 μmol g^{-1}. The larger band gap (3.2 eV) and rapid electron hole-pair recombination are responsible for the poor catalytic activity. Due to the simultaneous deposition of Cu^{2+} ions from $CuCl_2$, methane production increased 4.5-fold. Further, the individual deposition of $Cu(CH_3COO)_2$ and CuO as Cu^{2+} ion sources elevated

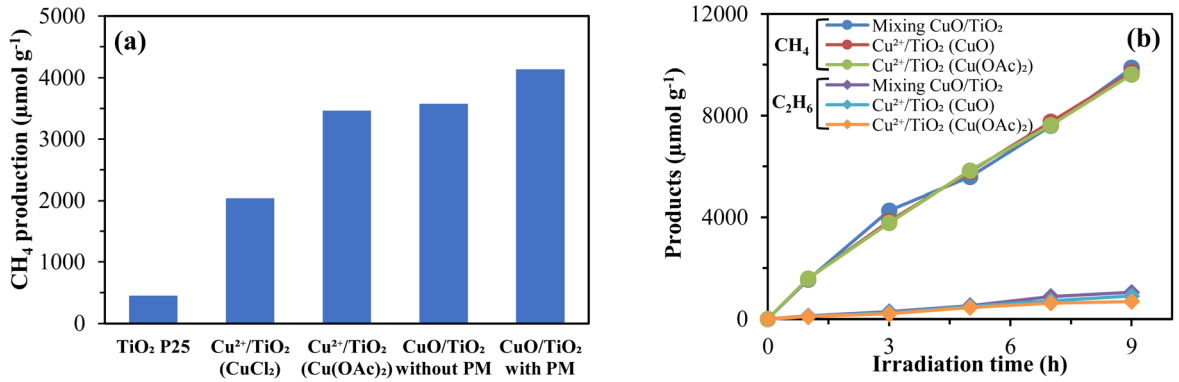

Fig. 1 (a) Effect of Cu sources on the photocatalytic methane production from acetic acid solution, and (b) comparison of hydrocarbon production rates under UV light (365 nm) irradiation.

methane production by 7.7 and 7.9 folds, respectively. 9.2 times enhanced methane was achieved from the physical mixing (PM) of CuO and TiO_2 compared to sole TiO_2. The redox potential of Cu^{2+} is 0.342 V *vs.* standard hydrogen electrode (SHE). It could be reduced by the photocatalyst when the CB of the semiconductor is more negative than the reduction potential of the Cu^{2+}.[42] The CB and VB edges for the TiO_2 photocatalyst are −0.46 V and + 2.7 V *vs.* SHE, respectively.[43] As a result, the photodeposition of Cu^{2+} on the TiO_2 surface generally occurred during the photocatalytic reaction and its metal reduction is also thermodynamically feasible.[44]

3.2. Comparison of hydrocarbon production rate under UV light irradiation

The comparison of hydrocarbon production rate using TiO_2 with simultaneous photodeposition of copper ions under UV/vis light irradiation with the extension of irradiation time was studied, as presented in Fig. 1b. The methane production rate gradually increased with the increase of irradiation time. All Cu^{2+} ion sources showed almost similar efficiency with or without physical mixing conditions. The physical mixing of CuO/TiO_2 showed little improvement in ethane production due to the favorable cyclic conversion of $CuO \rightarrow Cu^{2+} \rightarrow Cu^{1+} \rightarrow Cu^0$. The metallic copper ($Cu^0$) further reacts with dissolved oxygen and regenerates the CuO, reaching a cyclic redox reaction (eqn (1) and (2)). Since it was observed that the simultaneous photodeposition of copper on the TiO_2 enhanced the photocatalytic methane production, optimal conditions such as Cu^{2+} ion concentration, acetic acid concentration and reaction pH were optimized.

3.3. Photocatalytic performance conditions

Numerous operational factors, including catalyst and co-catalyst loading, substrate initial concentration and reaction pH, can affect the photocatalytic redox reaction. The following factors were optimized to achieve the maximum methane production under 12 h of UV/vis light illumination at 50 °C, whereas $Cu(OAc)_2$ was used as a Cu^{2+} ion source throughout the optimization reactions.

3.3.1. Effect of Cu^{2+} ion concentration. The effect of the co-catalyst (Cu^{2+}) concentration on the photocatalytic hydrocarbon production activity using TiO_2 with simultaneous deposition of Cu under UV/vis light irradiation was investigated (Fig. S1a†). Various amounts of Cu^{2+} were simultaneously introduced into the acetic acid solution along with the TiO_2 to determine the impact of co-catalyst loading on the photocatalytic hydrocarbon production rate with constant stirring conditions. The insertion of Cu^{2+} on the TiO_2 disclosed improved photocatalytic performance. The work function value of Cu (4.65 eV) is larger than the work function of TiO_2 (4.50 eV). A larger work function of metal ions is favorable for forming the Schottky junction effect at the metal-TiO_2 interface. As a result, metal with appropriate work functions can facilitate electron transfer, assist in overcoming the Schottky energy barrier and enhance photocatalytic efficiency.[44–46] Experimental results indicated that methane production gradually increased with the increase of Cu^{2+} concentration, reaching a maximum of 5.6 mg L^{-1} (0.45 wt% of Cu^{2+} relative to the weight of TiO_2), achieving the highest methane production (4136 μmol g^{-1}). The further increase of Cu^{2+} loading decreased the methane production due to the coagulation of Cu^{2+} and the incident light blockage on the photocatalyst surface.[47]

3.3.2. Effect of CH_3COOH concentration. In the photodegradation of organic compounds, the degradation rate increases to a certain point due to the rise of reactant concentration. The effect of acetic acid concentration on Cu/TiO_2 photocatalytic hydrocarbon production was studied under UV/vis light irradiation (Fig. S1b†). The amount of methane production sharply increased with the increase in acetic acid concentration from 0 to 1.0 mol L^{-1}. However, the highest amount (4730 μmol g^{-1}) of methane was evolved at 2.0 mol L^{-1} concentration of acetic acid, further increase of the reactant concentration, the production became steady due to the excess adsorption of acetic acid on the Cu/TiO_2 photocatalyst and reached saturation level.[48] With an increase of the initial concentration of acetic acid from 1.0 mol L^{-1} to 2.0 mol L^{-1}, the methane production rate was not so high compared to the concentration, which resulted in 1.0 mol L^{-1} being considered

the optimum concentration and all the further experiments were carried out accordingly.

3.3.3. Effect of reaction pH. The pH of the reaction medium and the charge on the catalyst's surface can affect the adsorption and dissociation of the reactant. The pH effect on Cu/TiO_2 photocatalytic hydrocarbon production was assessed by varying the pH from 1.5 to 3.5 (Fig. S1c†). 0.1 M HCl and 0.1 M NaOH reagents were used for the pH adjustment. The point zero charge (PZC) of TiO_2 P25 was approximately pH = 5.2 and the photocatalyst surface became chargeless at PZC and had no interaction with polar substances like acetic acid.[49] The photocatalytic degradation process is influenced by the PZC of TiO_2 and the dissociation constant (pK_a) of acetic acid (pK_a = 4.76). The surface of TiO_2 becomes positively and negatively charged when the pH is less and more than pH_{PZC}, respectively. At lower pH ($pH < pK_a$), acetic acid remains unchanged and at relatively higher pH ($pH > pK_a$), CH_3COO^- ions were produced. When $pH > pH_{PZC}$, the TiO_2 surface is negatively charged and the adsorption of CH_3COO^- ions on TiO_2 surface is difficult because of static repulsion.[47,50] Herein, due to the increase of reaction pH from 1.5 to 2.5, the methane production sharply increased from 36 μmol g^{-1} to 4136 μmol g^{-1}. With a further increase in pH from 3.5, the methane production rapidly decreased from 4136 μmol g^{-1} to 1886 μmol g^{-1}. Numerous investigations have demonstrated the crucial effect of reaction pH and charge on the photocatalyst surface, which can significantly affect the degradation of different carboxylic acids.[47]

3.4. Effect of irradiation time

The effect of irradiation time on Cu/TiO_2 photocatalytic hydrocarbon and hydrogen production from aqueous acetic acid solution was studied under UV/vis light irradiation (Fig. 2a). The amount of hydrocarbon production increased with the increase in irradiation time. In particular, CH_4 and C_2H_6 production sharply increased up to 30 h and 28 h (Fig. 2a, and S2a†), respectively. Further, the methane production remains steady till 96 h of irradiation. At the beginning of the reaction, in the presence of the optimal amount of dissolved oxygen, the number of electrons decreased, which was utilized for proton reduction, induced hydrocarbon production and reduced hydrogen generation. As a result, hydrogen production increased sharply after 32 h of continuous irradiation (Fig. S2b†). Meanwhile, oxygen in the system decreased sharply. The metal Cu^0 had been photo-precipitated on the TiO_2 surface due to the shortage of oxygen (Fig. S3†). As a result, methane and ethane production continued to increase until about 30 h but leveled off after the oxygen disappeared. The role of O_2 consumption during the Cu/TiO_2 photocatalytic reaction favored hydrocarbon production and reduced hydrogen generation (Fig. S2c†). Herein, CuO dissolves in the acetic acid aqueous solution and exists as Cu^{2+} ions. The Cu^{2+} ions were first reduced to metallic Cu^0 on the TiO_2 surface by reacting with the photogenerated electrons (eqn (1)). However, no discoloration was observed after 24 h of UV light irradiation. After 48 h of irradiation, the discoloration occurred due to the complete photo-precipitation of metallic Cu on the TiO_2 surface, which suggests no existence of dissolved oxygen in the reaction system (Fig. S3b†). The Fermi level can be induced toward greater negative potentials using Cu nanoparticles, which can store photogenerated electrons.[51] Therefore, it was assumed that the photo-precipitated metallic Cu was also dissolved in the acetic acid aqueous solution. To observe this, a considerable amount of metallic Cu powder was dissolved in the acetic acid solution and continuously stirred for 8 h at 50 °C, where a prolonged dissolution rate was observed (Fig. S3a†).[52] Therefore, in this system, the proportion of Cu metal directly dissolved in the aqueous acetic acid solution was tiny and it was considered that the Cu metal reacted with oxygen in the system and was oxidized to CuO (eqn (2)) before being dissolved in the aqueous acetic acid solution.[53] Further, the color change of the solution was compared before and after the reaction. In addition, the discolored solution returned to its initial color by introducing atmospheric oxygen into the reaction system for 3 h at 50 °C at continuous stirring conditions (Fig. S3b†).

$$Cu^{2+} + e^- \rightarrow Cu^+ + e^- \rightarrow Cu^0 \quad (1)$$

$$Cu + O_2 \rightarrow CuO \quad (2)$$

Therefore, it was considered that the metal Cu was oxidized to CuO again and dissolved in the aqueous acetic acid solution. It re-exists as Cu^{2+} ions; this conversion was hampered due to

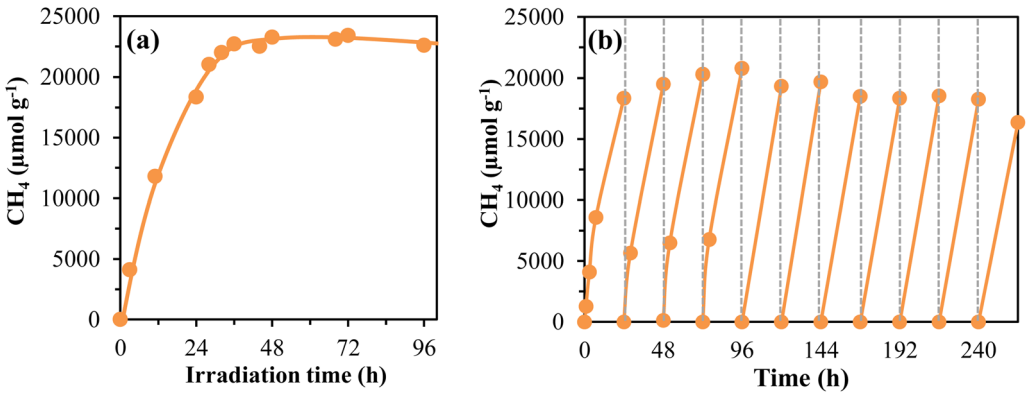

Fig. 2 (a) Effect of irradiation time on Cu/TiO_2 photocatalytic CH_4 production, and (b) stability test results of CH_4 production.

the absence of oxygen (Fig. S3c†). From the GC-TCD analysis, the oxygen in the system completely disappeared in about 30 h of illumination (Fig. S2c†). The solution began to change color almost at the same time. Therefore, oxygen plays a vital role in this system. Methane and ethane production continued to increase until about 30 h and finally leveled off after the complete vanishing of oxygen.

3.5. Reusability and stability test

To assess the stability and reusability of the Cu/TiO_2 photocatalysts, the hydrocarbon and hydrogen production from the acetic acid solution was carried out for eleven consecutive cycles (Fig. 2b and S4†). The reactor was fully evacuated before starting a new cycle. The photocatalytic methane production slightly increased till the fourth cycle due to the proper catalytic activation. Further, the production remained almost unchanged till the tenth cycle compared to the first cycle (Fig. 2b). For the ethane production (Fig. S4a†), a slight decrease was observed till the fifth cycle and a further slight elevation was found and became almost the same as the first cycle, indicating the excellent catalytic durability and reusability of Cu/TiO_2.[54] Compared to the first cycle, hydrogen production improved catalytic performance until the last cycle (Fig. S4b†). As mentioned earlier; oxygen favored the oxidation of acetic acid to produce methane. Every cycle consumed almost the same amount of oxygen and became near zero in 24 h of Cu/TiO_2 photocatalytic reaction (Fig. S4c†) for hydrocarbon production.

3.6. Visible light-driven methane production with Cu/TiO_2

The photocatalytic methane production from aqueous acetic acid solution utilizing TiO_2 with simultaneous photodeposition of Cu from different sources (CuO, $CuCl_2$ and $Cu(CH_3COO)_2$) was studied under visible light irradiation (405 nm) to explore the visible light response. The DRS result (Fig. 6a) proved that the simultaneous deposition of Cu on TiO_2 has increased the light absorption ability of Cu/TiO_2 than the pure TiO_2. No methane was detected from the photolysis of acetic acid. Similarly, no methane was tranced from the photocatalytic reaction of CuO due to its smaller band gap (1.2 eV) and faster electron–hole pair recombination rate.[55] Due to the large bandgap (3.2 eV), pure TiO_2 works better under ultraviolet light region only. Herein, a small amount of methane (0.4 μmol g^{-1}) was achieved from the photocatalytic reaction of pure TiO_2 P25 due to the less activation under visible light irradiation and fast undesirable electron–hole pair recombination. The deposition of specific metals on the TiO_2 surface significantly improved its photocatalytic efficiency.[56,57] The same amount of methane (0.4 μmol g^{-1}) was obtained from the catalytic reaction of CuO/TiO_2. Furthermore, using $CuCl_2$ as a Cu^{2+} ion source increased the photocatalytic methane production by 3.5-fold compared to pure TiO_2. The prior physical mixing of CuO/TiO_2 does not influence methane production due to the physical condition of CuO. However, the formation of Cu^{2+} ion and further reduction to metallic Cu^0 occurs inside the aqueous solution of acetic acid. The highest amount of methane (29 times compared to TiO_2 P25) was obtained using $Cu(OAc)_2$ as a copper ion supplier in simultaneous Cu deposition on TiO_2. The physical state and dissociation rate of $Cu(OAc)_2$ responded better than that of CuO and $CuCl_2$ under visible light irradiation.

3.7. Comparison of hydrocarbon production rate under visible light irradiation

The photocatalytic hydrocarbon production rate from the acetic acid solution under visible light irradiation using TiO_2 with simultaneous deposition of Cu^{2+} was also investigated. The Cu^{2+}/TiO_2 (CuO) photocatalytic methane production (39 μmol g^{-1}) was relatively higher than that of the physical mixing (32 μmol g^{-1}) condition (Fig. 3b). Moreover, the highest production (2.4 times of CuO/TiO_2) was obtained using Cu^{2+}/TiO_2 ($Cu(OAc)_2$) photocatalysts under the same conditions. The co-catalytic performance of CuO was relatively lower than $Cu(OAc)_2$ due to the lower solubility and dissociation. It's considered to produce more hydroxyl ions when dissolved in an aqueous acetic acid solution and the photogenerated holes are occupied by hydroxyl radicals. On the other hand, copper acetate behaves the opposite way and works smoothly under visible light irradiation due to its relatively faster dissociation.[58] Meanwhile, a trace amount of ethane was also detected at the mentioned conditions.

3.8. Characterization

3.8.1. XPS analysis. XPS studies were performed to investigate the surface chemical composition and electronic state of

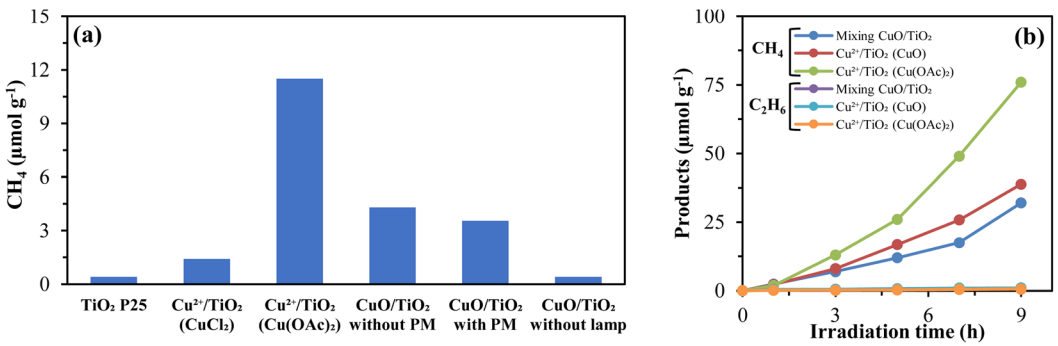

Fig. 3 (a) Effect of Cu sources on the photocatalytic methane production from acetic acid solution, and (b) comparison of hydrocarbon production rates under visible light (405 nm).

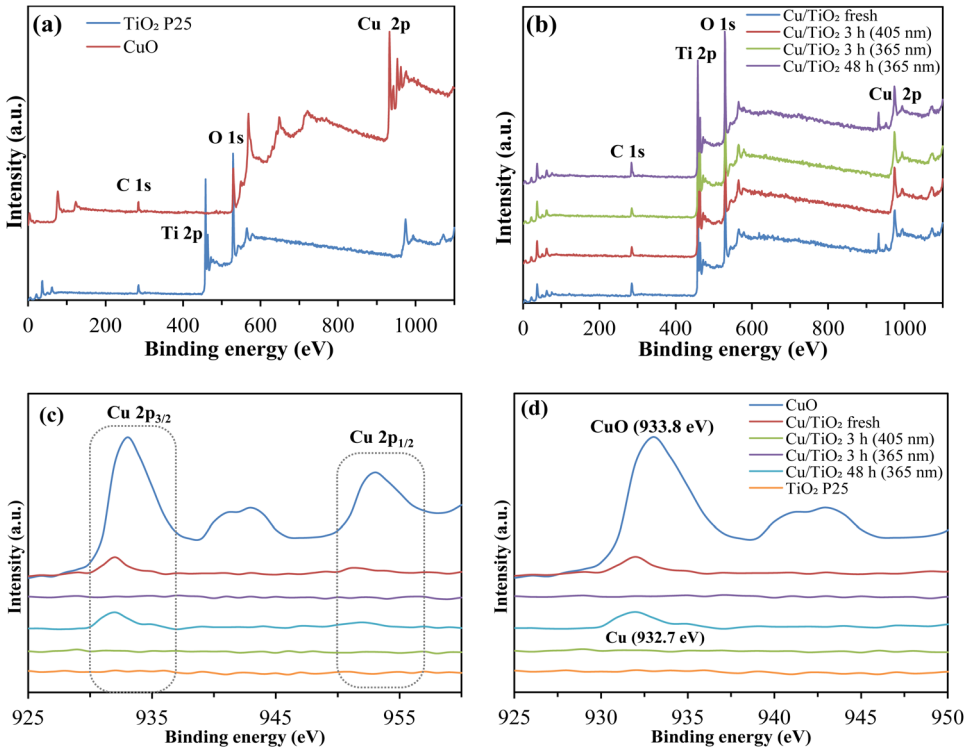

Fig. 4 XPS (a and b) survey spectra and high-resolution spectra of the studied catalysts (c) in the region of Cu 2p and (d) binding energy at varied conditions.

Cu/TiO_2. The survey and high-resolution spectra of Cu 2p of the studied catalyst are presented in Fig. 4a–d and the binding energy is depicted in Table S2.† From the experimental results (Fig. 4c), two characteristic peaks for Cu $2p_{3/2}$ and Cu $2p_{1/2}$ were detected at 933.8 eV and 953 eV, respectively, corresponding to Cu^{2+} (Fig. 4, Table S2†). A satellite peak was observed at 942 eV, indicating the presence of divalent Cu, which was seen in the pure CuO but considerably smaller in the fresh CuO/TiO_2 due to the low content of Cu.[59] After 3 h of irradiation by UV (365 nm) and visible (405 nm) light, no Cu compound was detected. However, the Cu $2p_{3/2}$ peak was re-existed at 932.7 eV after 48 h of UV irradiation. During the simultaneous photodeposition of CuO into the aqueous acetic acid solution, Cu^{2+} ions first form following the dissolution process. It further reduced to metallic Cu^0 on the TiO_2 surface by reacting with the photogenerated electrons (eqn (1)). Further, Cu^0 is oxidized to CuO by reacting with the dissolved oxygen and dissolved in the aqueous acetic acid solution and re-exists as Cu^{2+} ions (Fig. S3c†), due to this cyclic conversion, at a certain point Cu ion was not detected. In addition, although CuO/TiO_2 was simply kneaded with CuO and TiO_2 in an agate mortar, the peak position of CuO shifted slightly to the lower energy side.[29,60] This is considered to be caused by interaction with TiO_2 due to kneading.

3.8.2. Morphological investigation. The morphological change of Cu/TiO_2 before and after the irradiation was characterized by TEM analysis. Fig. 5a depicts the formation of a nanocluster of loaded Cu^{2+} on the surface of TiO_2.[61] In contrast, after 3 h of UV (365 nm) light radiation, the nanostructure of CuO notably decreased. A small amount of fragmented Cu^{2+} nanoparticles were detected around the surface edge of TiO_2 (Fig. 5b).[62,63]

3.8.3. BET analysis. To check the specific surface area and pore structure, the N_2 adsorption–desorption isotherms of the catalysts were measured at 77 K. Fig. S5(a–d)† depicted the N_2 adsorption–desorption isotherms of TiO_2 and Cu/TiO_2 before and after the irradiation. The effect of load Cu^{2+} on the surface area of TiO_2 was investigated. All the catalysts were classified as type IV in the IUPAC adsorption–desorption isotherm classification and there are H3-type hysteresis loops were found between $P/P_0 = 0.6$ and $P/P_0 = 1$. It is proven that the tested catalysts are mesoporous materials.[64,65] Table S1† illustrates the surface area and pore structure parameters of tested catalysts.[66] The irradiation decreased the BET surface area, total pore volume and average pore diameter. Though the pore volume and diameter gradually reduced with the increase in irradiation time, the BET surface area remained unchanged after 3 and 48 hours of irradiation (Table S1†).

3.8.4. DRS analysis. The light-harvesting capability of the following catalysts was characterized by ultraviolet-visible diffuse reflectance spectrum (DRS) analysis. From the "Kubelka–Munk (K–M)" transformation (Fig. 6a), CuO/TiO_2 showed absorption in the visible region before the irradiation due to the presence of CuO (inset).[67] CuO can absorb light of broad wavelengths but has no significant photocatalytic activity due to a smaller bandgap. After the irradiation (3–48 h), the catalyst had almost no absorption in the visible region. Still, the absorption in the ultraviolet region was significantly higher than that of the before irradiation.

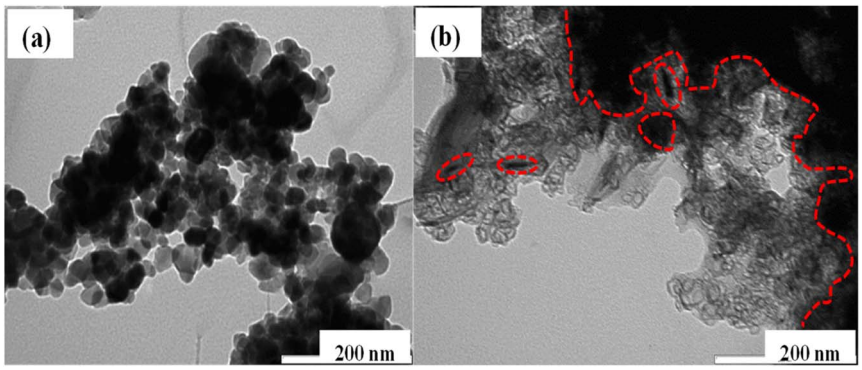

Fig. 5 TEM images of Cu/TiO_2 (a) before and (b) after 3 hours of irradiation.

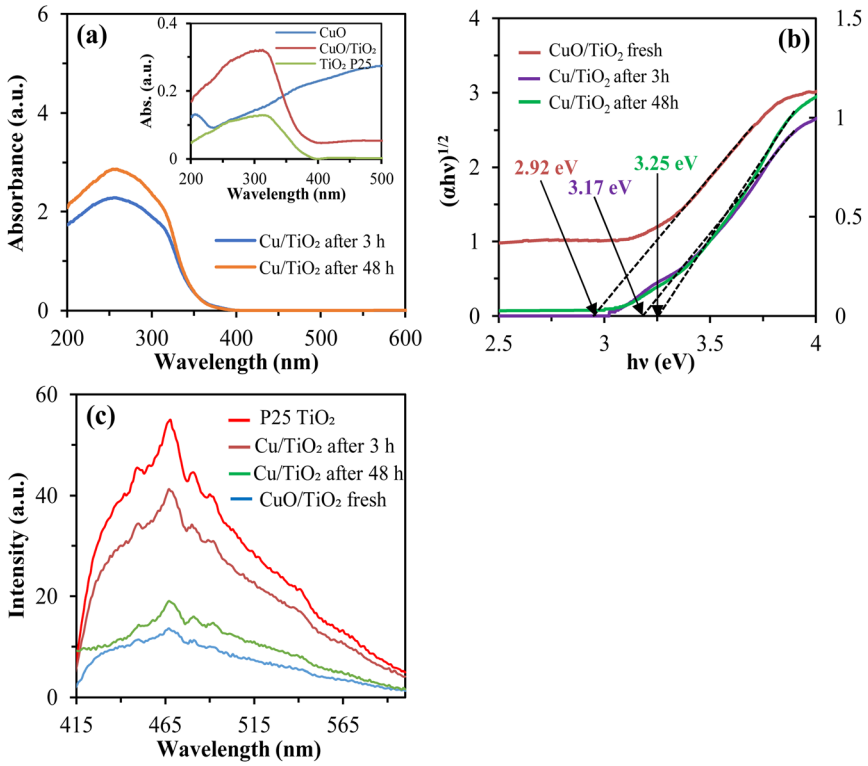

Fig. 6 (a) DRS spectra, (b) Tauc-plot and (c) PL spectra of the studied catalysts.

Further, the Tauc equation was implemented to calculate the energy bandgap as follows;

$$\alpha h\nu = A(h\nu - E_g)^n \quad (3)$$

$$(\alpha h\nu)^{1/n} = A(h\nu - E_g) \quad (4)$$

where α denotes the absorption coefficient, h is the Planck constant, ν is the light frequency, A is the characteristic constant and E_g is the bandgap energy, respectively. Electronic inter-band excitation helps to determine the transition steps; when $n = 1/2$, it depicts the direct transition and $n = 2$ stands for the indirect transition, respectively. For anatase-type titanium oxide, $n = 2$ is set because the inter-band excitation is an indirect transition.[68] From eqn (4), the bandgap energy can be obtained by plotting $(\alpha h\nu)^{1/n}$ on the vertical axis and $h\nu$ on the horizontal axis and extrapolating a straight line (Fig. 6b). Where the energy band gap of fresh CuO/TiO_2 was found 2.92 eV, which indicating the Cu deposition on the TiO_2 surface significantly reduced the bandgap. Further, the energy band gap of Cu/TiO_2 was increased to 3.17 eV and 3.25 eV after 3 h and 48 h of light irradiation, which indicates the state change of Cu due to the photocatalytic reaction.

3.8.5. PL analysis. The photoluminescence (PL) spectral technique was utilized to examine the catalysts' electron hole-pair separation and migration efficiency. The smaller peak of the photoluminescence spectrum indicates the suppression of the recombination of photogenerated electron–hole pairs. From

the experimental results (Fig. 6c), the recombination of electrons and holes is considerably capable of suppressing CuO/TiO_2 before irradiation compared to P25 TiO_2. Comparing the catalyst after 3 h and 48 h irradiation, the peak was smaller in the sample after 48 h irradiation, suggesting that more metallic Cu^{2+} was photo-deposited on the TiO_2 surface and delayed the recombination rate. The possible reasons for the improved photocatalytic activity of Cu/TiO_2 are either increasing light absorption or effectively capturing the photoinduced electrons due to the proper amount of oxygen vacancies and Cu ions on the TiO_2 surface. Where Cu ions can work as electron traps to reduce the recombination rate of h^+/e^- pairs (eqn (1)). Therefore, both Cu^{2+} and Cu^+ ions are able of accepting the photogenerated electrons.[69]

3.9. Photocatalysis mechanism

To better understand the simultaneous Cu-deposition on the TiO_2 in photocatalytic hydrocarbon and hydrogen production from acetic acid solution, a possible reaction mechanism has been proposed combining the mentioned theories and experimental consequences (Fig. 7). Electron transfer to the conduction band of CuO is feasible due to its location just below the conduction band of TiO_2 under the UV light irradiation. For the same reason, the hole transfer from TiO_2's valence band to CuO's valence band is permitted and the combined effect of Cu/TiO_2 increases hydrocarbon and hydrogen production.[36] When light energy larger than the TiO_2 bandgap is absorbed by the TiO_2 semiconductor, the photogenerated electrons move toward the conduction band, resulting in photogenerated holes becoming available in the valence band (eqn (5)). The photogenerated electrons are used to reduce Cu^{2+} ions into metals in the aqueous acetic acid solution and metallic Cu is deposited on the TiO_2 surface. Since electrons are consumed one after another, it is considered that the oxidation reaction by holes is accelerated. The photo-precipitated Cu metal is oxidized by dissolved oxygen in the system to become CuO (eqn (2) and Fig. S3c†), further dissolved in an acetic acid aqueous solution and re-existed as Cu^{2+} ions. As long as oxygen exists in the system, this cycle always causes the precipitation of fresh metal Cu so that the photocatalytic activity can be maintained semi-permanently.

Next, the oxidation reaction mechanism of acetic acid considered in this experiment is shown below (Scheme 1 and Fig. 7b–f). Where the photogenerated holes and $^{\bullet}OH$ radicals are influenced by the rate of water-splitting (eqn (6)). Further, the adsorbed CH_3COOH dissociates to CH_3COO^- and comes into contact with the photogenerated holes to produce $^{\bullet}CH_3$ and CO_2, followed by the Photo-Kolbe reaction (eqn (7) and (8)). At this stage, $^{\bullet}CH_3$ radicles react with water to release CH_4 and with another $^{\bullet}CH_3$ to produce C_2H_6 (eqn (9) and (10)). Methanol (CH_3OH), formaldehyde (HCHO) and formic acid (HCOOH) were detected in the liquid phase during the photocatalytic decomposition of acetic acid.[27] The photogenerated hole reacts with the methanol to produce formaldehyde (eqn (11) and (12)) and further formic acid was detected as an intermediate due to the oxidation reaction in the presence of $^{\bullet}OH$ and hole (eqn (13)). Finally, the formate ion comes in contact with photogenerated holes and produces H^+, which is further reduced by the photogenerated electron to evolve H_2 (eqn (15)).

Next, the effects of dissolved oxygen and hydroxide ions on the generation of hydrogen and hydrocarbons were considered. Since the reduction potential of oxygen is on the nobler side

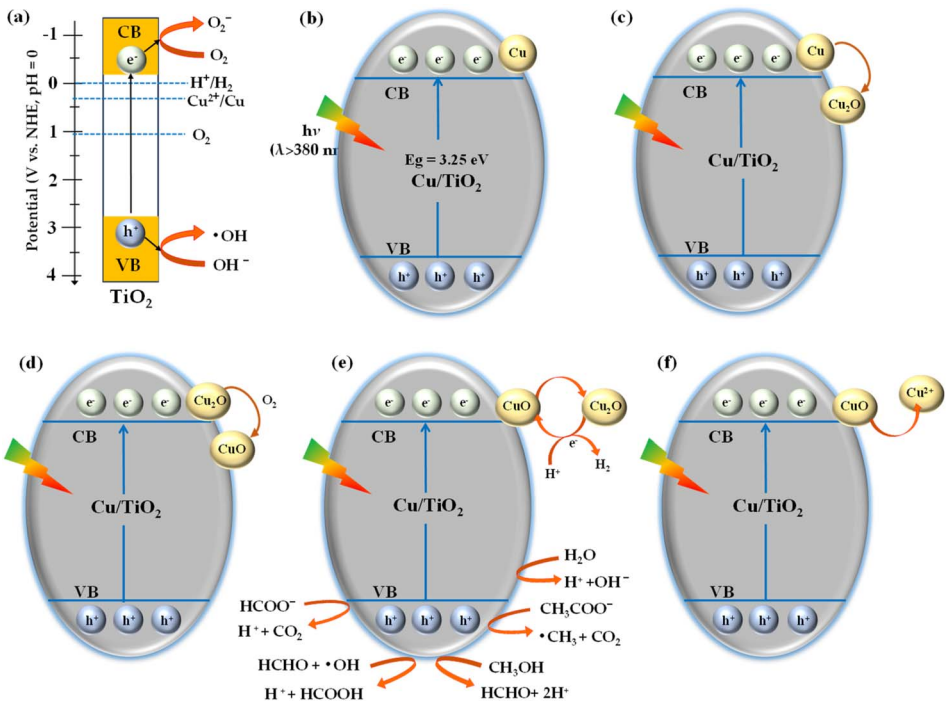

Fig. 7 Mechanism for (a) oxygen reduction, and hydroxide ion oxidation and (b–f) photocatalytic hydrocarbon and H_2 production.

$$Cu/TiO_2 + h\nu \rightarrow h^+ (TiO_2) + e^- (Cu) \quad (5)$$
$$h^+ + H_2O \rightarrow H^+ + {}^\bullet OH \quad (2H^+ + 2e^- \rightarrow H_2) \quad (6)$$
$$CH_3COOH \rightarrow CH_3COO^- + H^+ \quad (7)$$
$$CH_3COO^- + h^+ \rightarrow {}^\bullet CH_3 + CO_2 \quad ({}^\bullet CH_3 + {}^\bullet OH \rightarrow CH_3OH) \quad (8)$$
$${}^\bullet CH_3 + H_2O \rightarrow CH_4 + {}^\bullet OH \quad (9)$$
$${}^\bullet CH_3 + {}^\bullet CH_3 \rightarrow C_2H_6 \quad (10)$$
$$CH_3OH + h^+ \rightarrow H^+ + {}^\bullet CH_2OH \quad (11)$$
$${}^\bullet CH_2OH + h^+ \rightarrow H^+ + HCHO \quad (H^+ + e^- \rightarrow 1/2H_2) \quad (12)$$
$$HCHO + {}^\bullet OH + h^+ \rightarrow H^+ + HCOOH \quad (13)$$
$$HCOOH \rightarrow HCOO^- \quad (14)$$
$$HCOO^- + 2\,h^+ \rightarrow H^+ + CO_2 \quad (H^+ + e^- \rightarrow 1/2H_2) \quad (15)$$

Scheme 1 Reaction mechanism for the hydrocarbon production from acetic acid.[47,70,71]

than the potential of the conduction band of TiO_2, dissolved oxygen is thought to be reduced using electrons photogenerated on titanium oxide to form superoxide anions. Therefore, when the amount of dissolved oxygen increases, the number of electrons used for proton reduction decreases, which is thought to harm hydrogen generation. In addition, it is believed that when the pH increases and the number of hydroxide ions increases, the methane produced decreases because the photogenerated holes are consumed and hydroxyl radicals are generated. The conduction band potential of TiO_2 is −0.2 V (Fig. 7b), which is more negative than the oxidation–reduction potential of Cu^{2+}/Cu of +0.34 V, so in this stage, Cu ions can be reduced to metallic Cu. A comparative TiO_2 photocatalytic methane production efficiency from acetic acid result is presented in Table S3.†

4. Conclusions

In summary, the photocatalytic activity of *in situ* Cu-deposited TiO_2 was studied for the hydrocarbon and hydrogen production from aqueous acetic acid solution under UV light irradiation. Factors that affect the photocatalytic reaction, such as substrate initial concentration, irradiation time, catalyst and co-catalyst dosage and reaction pH were optimized. The structural and optical properties of Cu/TiO_2 were characterized by XPS, TEM, BET surface area, DRS and PL analysis. The appropriate work function of Cu contributed to Schottky junction formation, which facilitates electron transfer, assists in overcoming the Schottky energy barrier and leads to enhanced photocatalytic efficiency. The energy band gap and light absorption capability of Cu/TiO_2 were significantly improved due to the Cu deposition. PL results confirm that the photogenerated charge separation and migration capability also improved for Cu/TiO_2. The optimized Cu/TiO_2 exhibited the highest methane production (4136 μmol g^{-1}), 9.2-fold more than pure TiO_2 without using any noble metal. The most straightforward technique reduced the recombination rate and energy band gap, resulting in the simultaneous production of hydrocarbon and hydrogen, which also smoothly proceeded under visible light (405 nm) irradiation and atmospheric conditions. Additionally, the excellent stability of Cu/TiO_2 was proven through cycling experiments. Finally, the Cu/TiO_2 can be considered a potential photocatalyst for efficiently converting solar power to chemical energy.

Data availabilty

The data that support this study's findings are available from the corresponding author upon reasonable request. Additionally, any ESI,† including figures and datasets generated during the study, will be provided in the ESI† section of the manuscript.

Author contributions

Monir Uzzaman: writing – original draft, writing – review & editing, investigation, formal analysis, methodology, visualization, data curation. Mai Furukawa: writing – review & editing. Ikki Tateishi: writing – review & editing. Hideyuki Katsumata: writing – review & editing, validation. Mst. Farhana Afrin: writing – review & editing, methodology. Satoshi Kaneco: conceptualization, supervision, methodology, validation, writing – review & editing.

Conflicts of interest

There are no conflicts to declare.

Acknowledgements

This research was partially funded by Grant-in-Aid for Scientific Research (B) 21H03642 from the Ministry of Education, Culture, Sports, Science and Technology of Japan.

References

1 R. Falkner, *Int. Aff.*, 2016, **92**, 1107–1125.
2 I. Dincer and C. Acar, *Int. J. Energy Res.*, 2015, **39**, 585–606.
3 G. Yadav and M. Ahmaruzzaman, *Inorg. Chem. Commun.*, 2022, **138**, 109288.
4 Y. Yang, C. Zhou, W. Wang, W. Xiong, G. Zeng, D. Huang, C. Zhang, B. Song, W. Xue and X. Li, *Chem. Eng. J.*, 2021, **405**, 126547.
5 P. V. Kamat, *J. Phys. Chem. C*, 2007, **111**, 2834–2860.
6 M. S. S. Danish, L. L. Estrella, I. M. A. Alemaida, A. Lisin, N. Moiseev, M. Ahmadi, M. Nazari, M. Wali, H. Zaheb and T. Senjyu, *Metals*, 2021, **11**, 80.
7 S. Mozia, A. Heciak and A. W. Morawski, *J. Photochem. Photobiol. A Chem.*, 2010, **216**, 275–282.
8 I. Paramasivam, H. Jha, N. Liu and P. Schmuki, *Small*, 2012, **8**, 3073–3103.
9 H. Park, Y. Park, W. Kim and W. Choi, *J. Photochem. Photobiol. C Photochem. Rev.*, 2013, **15**, 1–20.
10 Z. Zhang, C.-C. Wang, R. Zakaria and J. Y. Ying, *J. Phys. Chem. B*, 1998, **102**, 10871–10878.
11 H. D. Jang, S.-K. Kim and S.-J. Kim, *J. Nano. Res.*, 2001, **3**, 141–147.
12 U. I. Gaya and A. H. Abdullah, *J. Photochem. Photobiol. C Photochem. Rev.*, 2008, **9**, 1–12.

13 N. Yahya, F. Aziz, N. A. Jamaludin, M. A. Mutalib, A. F. Ismail, W. N. W. Salleh, J. Jaafar, N. Yusof and N. A. Ludin, *J. Environ. Chem. Eng.*, 2018, **6**, 7411–7425.
14 K. Nishijima, B. Ohtani, X. Yan, T. Kamai, T. Chiyoya, T. Tsubota, N. Murakami and T. Ohno, *Chem. Phys.*, 2007, **339**, 64–72.
15 M. Anpo and M. Takeuchi, *J. Catal.*, 2003, **216**, 505–516.
16 B. Kraeutler and A. J. Bard, *J. Am. Chem. Soc.*, 1978, **100**, 2239–2240.
17 H. Tong, S. Ouyang, Y. Bi, N. Umezawa, M. Oshikiri and J. Ye, *Adv. Mater.*, 2012, **24**, 229–251.
18 C. He, D. Shu, M. Su, D. Xia, M. Abou Asi, L. Lin and Y. Xiong, *Desalination*, 2010, **253**, 88–93.
19 G. Colón, M. Maicu, M. C. s Hidalgo and J. A. Navío, *Appl. Catal., B*, 2006, **67**, 41–51.
20 X.-J. Zheng, L.-F. Wei, Z.-H. Zhang, Q.-J. Jiang, Y.-J. Wei, B. Xie and M.-B. Wei, *Int. J. Hydrogen Energy*, 2009, **34**, 9033–9041.
21 M. A. Barakat, H. Schaeffer, G. Hayes and S. Ismat-Shah, *Appl. Catal., B*, 2005, **57**, 23–30.
22 J. Serafin, M. Ouzzine, J. Sreńscek-Nazzal and J. Llorca, *J. Photochem. Photobiol. A Chem.*, 2022, **425**, 113726.
23 S. Asal, M. Saif, H. Hafez, S. Mozia, A. Heciak, D. Moszyński and M. S. A. Abdel-Mottaleb, *Int. J. Hydrogen Energy*, 2011, **36**, 6529–6537.
24 Z. H. N. Al-Azri, W.-T. Chen, A. Chan, V. Jovic, T. Ina, H. Idriss and G. I. N. Waterhouse, *J. Catal.*, 2015, **329**, 355–367.
25 S. Mozia, A. Heciak and A. W. Morawski, *Appl. Catal., B*, 2011, **104**, 21–29.
26 S. Mozia, A. Heciak, D. Darowna and A. W. Morawski, *J Photochem. Photobiol. A Chem.*, 2012, **236**, 48–53.
27 S. Mozia, A. Heciak and A. W. Morawski, *Catal. Today*, 2011, **161**, 189–195.
28 A. Heciak, A. W. Morawski, B. Grzmil and S. Mozia, *Appl. Catal., B*, 2013, **140**, 108–114.
29 A. Amorós-Pérez, L. Cano-Casanova, M. Á. Lillo-Ródenas and M. C. Román-Martínez, *Catal. Today*, 2017, **287**, 78–84.
30 L. M. Betts, F. Dappozze and C. Guillard, *Appl Catal, A*, 2018, **554**, 35–43.
31 Y. Cao, S. N. Lou and T. Ohno, *Mater. Lett.*, 2023, **347**, 134552.
32 K. Nakata and A. Fujishima, *J. Photochem. Photobiol. C Photochem. Rev.*, 2012, **13**, 169–189.
33 A. Madhumitha, V. Preethi and S. Kanmani, *Int. J. Hydrogen Energy*, 2018, **43**, 3946–3956.
34 D. Guerrero-Araque, P. Acevedo-Peña, D. Ramírez-Ortega, L. Lartundo-Rojas and R. Gómez, *J. Chem. Technol. Biotechnol.*, 2017, **92**, 1531–1539.
35 S. Chen, Q. Shi, Z. Xue, X. Sun and W. Xiang, *Int. J. Hydrogen Energy*, 2011, **36**, 8915–8926.
36 T. Miwa, S. Kaneco, H. Katsumata, T. Suzuki, K. Ohta, S. Chand Verma and K. Sugihara, *Int. J. Hydrogen Energy*, 2010, **35**, 6554–6560.
37 A. Pérez-Larios, R. Lopez, A. Hernández-Gordillo, F. Tzompantzi, R. Gómez and L. M. Torres-Guerra, *Fuel*, 2012, **100**, 139–143.
38 C. Wang, X. Cai, Y. Chen, Z. Cheng, X. Luo, S. Mo, L. Jia, P. Lin and Z. Yang, *Chem. Eng. J.*, 2017, **317**, 522–532.
39 Md. T. Uddin, Y. Nicolas, C. Olivier, W. Jaegermann, N. Rockstroh, H. Junge and T. Toupance, *Phys. Chem. Chem. Phys.*, 2017, **19**, 19279–19288.
40 M. Muscetta, R. Andreozzi, L. Clarizia, I. Di Somma and R. Marotta, *Int. J. Hydrogen Energy*, 2020, **45**, 28531–28552.
41 G. Li, J. Huang, J. Chen, Z. Deng, Q. Huang, Z. Liu, W. Guo and R. Cao, *ACS Omega*, 2019, **4**, 3392–3397.
42 D. R. Lide, *CRC Handbook of Chemistry and Physics*, CRC Press, 2004, vol. 85.
43 T. Aarthi and G. Madras, *Catal. Commun.*, 2008, **9**, 630–634.
44 P. Gomathisankar, D. Yamamoto, H. Katsumata, T. Suzuki and S. Kaneco, *Int. J. Hydrogen Energy*, 2013, **38**, 5517–5524.
45 H. B. Michaelson, *J. Appl. Phys.*, 1977, **48**, 4729–4733.
46 T. Ano, F. Kishimoto, S. Tsubaki, Y.-H. Lu, J. N. Hohman, M. M. Maitani, M. Salmeron and Y. Wada, *J. Phys. Chem. C*, 2021, **125**, 13984–13989.
47 M. Uzzaman, M. F. Afrin, M. Furukawa, I. Tateishi, H. Katsumata and S. Kaneco, *ChemEngineering*, 2024, **8**, 75.
48 M. H. Suhag, I. Tateishi, M. Furukawa, H. Katsumata, A. Khatun and S. Kaneco, *ChemEngineering*, 2022, **6**, 43.
49 M. Zeng, *Bull. Korean Chem. Soc.*, 2013, **34**, 953–956.
50 E. N. Bakatula, D. Richard, C. M. Neculita and G. J. Zagury, *Environ. Sci. Pollut. Res.*, 2018, **25**, 7823–7833.
51 P. Gomathisankar, K. Hachisuka, H. Katsumata, T. Suzuki, K. Funasaka and S. Kaneco, *Int. J. Hydrogen Energy*, 2013, **38**, 11840–11846.
52 G. Li, N. M. Dimitrijevic, L. Chen, T. Rajh and K. A. Gray, *J. Phys. Chem. C*, 2008, **112**, 19040–19044.
53 X. J. Zheng, Y. J. Wei, L. F. Wei, B. Xie and M. B. Wei, *Int. J. Hydrogen Energy*, 2010, **35**, 11709–11718.
54 K. Rajendran, M. Sharma, A. Jaison, M. Ankitha, A. D. Tiwari, C. P. Vinod and D. Jagadeesan, *Catal. Sci. Technol.*, 2023, **13**, 2330–2339.
55 P. C. Okoye, S. O. Azi, T. F. Qahtan, T. O. Owolabi and T. A. Saleh, *Mater. Today Chem.*, 2023, **30**, 101513.
56 L. Xu, G. Zheng, S. Pei and J. Wang, *Optik*, 2018, **158**, 382–390.
57 K. Nagaveni, M. S. Hegde, N. Ravishankar, G. N. Subbanna and G. Madras, *Langmuir*, 2004, **20**, 2900–2907.
58 T. Aguilar, J. Navas, R. Alcántara, C. Fernández-Lorenzo, J. J. Gallardo, G. Blanco and J. Martín-Calleja, *Chem. Phys. Lett.*, 2013, **571**, 49–53.
59 B. Srinivas, B. Shubhamangala, K. Lalitha, P. Anil Kumar Reddy, V. Durga Kumari, M. Subrahmanyam and B. R. De, *Photochem. Photobiol.*, 2011, **87**, 995–1001.
60 B. Xin, P. Wang, D. Ding, J. Liu, Z. Ren and H. Fu, *Appl. Surf. Sci.*, 2008, **254**, 2569–2574.
61 A. Moghanian, F. Sharifianjazi, P. Abachi, E. Sadeghi, H. Jafarikhorami and A. Sedghi, *J. Alloys Compd.*, 2017, **698**, 518–524.
62 Y. Gao and S. A. Elder, *Mater. Lett.*, 2000, **44**, 228–232.
63 S. Xu and D. D. Sun, *Int. J. Hydrogen Energy*, 2009, **34**, 6096–6104.

64 M. Thommes, K. Kaneko, A. V. Neimark, J. P. Olivier, F. Rodriguez-Reinoso, J. Rouquerol and K. S. W. Sing, *Pure Appl. Chem.*, 2015, **87**, 1051–1069.
65 M. Uzzaman, M. H. Suhag, H. Katsumata, I. Tateishi, M. Furukawa and S. Kaneco, *Catal. Sci. Technol.*, 2024, **14**, 267–278.
66 L. Liu, F. Gao, H. Zhao and Y. Li, *Appl. Catal., B*, 2013, **134–135**, 349–358.
67 W. E. Vargas and G. A. Niklasson, *Appl. Opt.*, 1997, **36**, 5580.
68 A. Dolgonos, T. O. Mason and K. R. Poeppelmeier, *J. Solid State Chem.*, 2016, **240**, 43–48.
69 B. Xin, P. Wang, D. Ding, J. Liu, Z. Ren and H. Fu, *Appl. Surf. Sci.*, 2008, **254**, 2569–2574.
70 X.-J. Zheng, L.-F. Wei, Z.-H. Zhang, Q.-J. Jiang, Y.-J. Wei, B. Xie and M.-B. Wei, *Int. J. Hydrogen Energy*, 2009, **34**, 9033–9041.
71 M. F. Afrin, M. Furukawa, I. Tateishi, H. Katsumata, M. Uzzaman and S. Kaneco, *J. Compos. Sci.*, 2025, **9**(2), 68.